THE ASTROPHYSICAL JOURNAL, 415:75–81, 1993 September 20


# MILLIMETER AND SUBMILLIMETER CONTINUUM EMISSION FROM EARLY-TYPE GALAXIES

MICHEL FICH
Harvard-Smithsonian Center for Astrophysics; and Guelph-Waterloo Program for Graduate Work in Physics, University of Waterloo, Waterloo, Ontario, Canada N2L 3G1

AND

PAUL HODGE
Astronomy Department, University of Washington, FM-20, Seattle, WA 98195
*Received 1992 December 28; accepted 1993 March 30*

## ABSTRACT

Twenty-two early-type galaxies that were detected by *IRAS* have been searched for continuum emission at millimeter and submillimeter wavelengths using the James Clerk Maxwell Telescope (JCMT). *IRAS* was relatively insensitive to cold dust that emits primarily at these longer wavelengths. In this first survey we were able to detect or achieve useful limits on the emission from 14 of the 22 galaxies observed. From these data we estimate upper limits on the dust temperature and lower limits on the mass of dust within the JCMT beam. These results are compared with H I and CO data and with the blue luminosities of the galaxies. The results are consistent with a model where the dust-to-gas ratio is similar to the Galactic one, and the amount of cold dust is an order of magnitude greater than the amount of warm dust (as is also seen in our Galaxy). The total dust mass, normalized to the luminosity of the entire galaxy, is much lower than is found in spiral galaxies, as expected.

*Subject headings:* dust, extinction — galaxies: elliptical and lenticular, cD — galaxies: ISM — infrared: galaxies — radio continuum: galaxies

## 1. INTRODUCTION

Classically, one of the defining characteristics of early-type galaxies is that they have no detectable interstellar medium. If, for example, an elliptical galaxy has obvious extinction due to interstellar dust, it is labeled "peculiar." However, there has been increasing evidence that many early-type galaxies perhaps more than half, contain detectable interstellar material of some kind. Since the environment within elliptical galaxies is quite different from that within spiral and irregular galaxies, elliptical galaxies provide an alternate "laboratory" for understanding the fundamental processes in interstellar media.

Dust is seen optically in many elliptical galaxies (e.g., Ebneter & Balick 1985); H I and CO have been detected in some (e.g., Knapp, Turner, & Cuniffe 1985; Lees et al. 1991); and in perhaps the most sensitive test, many ellipticals appear to be *IRAS* sources at 60 and 100 μm (Jura 1986; Knapp et al. 1989). A compilation of virtually all observations of interstellar matter in early-type galaxies has recently been produced by Roberts et al. (1991). Bregman, Hogg, & Roberts (1992) discuss the trends evident in this compilation.

The *IRAS* observations of dust in early-type galaxies show that dust is common, but fails to provide a good estimate of the mass and temperature of the dust. Unfortunately, *IRAS* was not sensitive to cold dust (dust with temperatures below ≈25 K). In our own Galaxy *IRAS* directly detects only 5%–10% of the dust because most of the dust is too cold to emit strongly in the mid-infrared (Cox & Mezger 1989; Young 1990). Instead, most of the emission from the dust is at submillimeter wavelengths.

In order to test the possibility that there might be significant amounts of cold dust in early-type galaxies, we have begun a program of observing a selected sample of them at submillimeter wavelengths with the James Clerk Maxwell Telescope[1] (JCMT). A preliminary project to test the feasibility of this project was carried out on the Local Group galaxy NGC 205 (Fich & Hodge 1991). NGC 205 has visible dust clouds near the center, and these were searched for continuum emission. Only marginal detections were found on each of the three dust clouds observed. However, the nucleus was detected although there was no a priori reason to expect dust emission there: the measured extinction (in larger apertures) did not show any significant optical extinction (Wilcots et al. 1990).

For this continuation of the project a set of early-type galaxies, especially elliptical galaxies, with large 100 μm flux density, and large ratios of 100 to 60 μm flux density were selected from the catalog of Knapp et al. (1989). In § 2 we present our first set of observations of these galaxies. The results of this preliminary survey are described in § 3, and some discussion of the significance of these results appears in § 4.

## 2. OBSERVATIONS

The data were obtained using the James Clerk Maxwell Telescope, a 15 m diameter submillimeter telescope located on Mauna Kea, Hawaii, and the UKT14 receiver during the period of 1991 November 8–10. The UKT14 detector is a liquid $^3$He–cooled composite Ge bolometer with a set of filters that cover each of the main atmospheric windows between 0.3 and 2 mm. A chopping secondary was used to reduce background noise and sky fluctuations. The beam separation was 60″ in azimuth for virtually all of our observations. A complete description of the UKT14 system is given by Duncan et al.

[1] The James Clerk Maxwell Telescope is operated by the Royal Observatory Edinburgh on behalf of the Science and Engineering Research Council of the United Kingdom, the Netherlands Organisation for Scientific Research, and the National Research Council of Canada.

(1990). Details of the telescope and other instrumentation can be found in Matthews (1990). Pointing was checked frequently (whenever the telescope was moved to a different source and at least once per hour if there was no substantial change in telescope position) by observing bright point sources in the JCMT pointing list. The pointing was accurate to better than 4″ in virtually every case.

Useful data were obtained at 450, 800, and 1100 μm. At these wavelengths, with the UKT14 65 mm aperture, the JCMT/UKT14 has a half-power beamwidth of 17″.7, 16″.5, and 18″.4, respectively. Measurements of the gain over the past few years have produced a range of values: here we use 16.0, 9.0. and 12.5 Jy $mV^{-1}$ for 450, 800, and 1100 μm, as suggested by the most recent measurements (1990 August 19; G. Sandell, private communication). The weather was reasonably good for submillimeter observations for much of the time, and so there was more emphasis on observing at the shorter wavelengths of 800 and 450 μm. Toward the end of the observing run, conditions worsened; the 450 μm observations were abandoned and the observing time was split betwen 800 and 1100 μm.

The only planet available as a primary flux calibrator was Uranus. On the first night it was assumed to be 1″.76 in diameter and assumed to have a total flux density in the 65 mm aperture of 68.2, 74.3, and 43.88 Jy at 450, 800, and 1100 μm. These values were determined by the program FLUXES available at the Joint Astronomy Centre, Hilo, and are based on models discussed by Griffin et al. (1986).

In order to measure and correct for the sky opacity, we observed at least four secondary calibrators at the beginning of each night and then again after each hour of taking data on our program sources. The calibrators used are listed in Table 1. Most of these were taken from the UKT14 calibrator list (1991 November 8 version). Our observations were generally consistent with the standard values of the calibrator flux densities. On average, the values determined from our data are within 1% at 450 μm, 2% at 800 μm, and 3% at 1100 μm. However, we found that the flux densities given for a few of these sources were inconsistent with our values. The objects showing the greatest difference between our values and the standard manual are VY CMa and OH 231.8. Our observation of VY CMa gives 0.52 ± 0.04 Jy at 1100 μm, while the standard value is 0.95 ± 0.09 Jy, a difference of 45%. Our measurements of OH 231.8 give higher fluxes than the calibrator manual in all three bands by 20%–30%.

TABLE 1

SUMMARY OF FLUXES ESTIMATED FOR SECONDARY CALIBRATORS

| Name | $S_\nu$(450 μm) (Jy) | $S_\nu$(800 μm) (Jy) | $S_\nu$(1100 μm) (Jy) |
|---|---|---|---|
| W3(OH) | 222.7 ± 6.0 | 32.4 ± 0.4 | 13.06 ± 0.07 |
| CRL 618 | 11.2 ± 0.9 | 4.2 ± 0.2 | 2.66 ± 0.03 |
| VY CMa | 8.6 ± 0.7 | 1.7 ± 0.1 | 0.52 ± 0.04 |
| OH 231.8 | 16.4 ± 0.5 | 3.7 ± 0.1 | 1.39 ± 0.03 |
| 16293 − 2422 | 146.5 ± 3.4 | 20.1 ± 0.4 | 7.83 ± 0.08 |
| G34.3 | 479.0 ± 8.7 | 69.5 ± 0.9 | 30.59 ± 0.41 |
| K3-50 | 91.5 ± 4.5 | 17.6 ± 0.1 | 9.40 ± 0.17 |
| W75N | 238.2 ± 4.5 | 33.9 ± 0.7 | 11.58 ± 0.22 |
| CRL 2688 | 23.4 ± 1.3 | 6.8 ± 0.2 | 2.71 ± 0.08 |
| NGC 7538 IRS 1 | 149.6 ± 9.2 | 22.0 ± 2.3 | 9.98 ± 0.56 |
| 3C 84 | 1.6 ± 0.3 | 1.8 ± 0.1 | 2.39 ± 0.03 |
| OJ 287 | 0.2 ± 0.3 | 2.0 ± 0.1 | 2.07 ± 0.04 |
| 3C 345 | 2.4 ± 0.6 | 4.3 ± 0.1 | 5.34 ± 0.02 |

Table 1 lists the flux density determined from our data for each secondary calibrator. The uncertainty quoted for each of our determinations is that estimated from the scatter within our measurements (i.e., it is an internal uncertainty) and does not include uncertainties due to other sources of error, such as the absolute scale of the flux density or pointing. An important source of further uncertainty is the choice of gain for each band as described above. Other possible sources of error include possible gain variations with differing source elevations, as has been occasionally reported for this instrument. We searched for this in our data but were unable to confirm this effect. We used our flux densities rather than those in the UKT14 calibrator list, to determine the sky opacities.

The sky opacity calculated from the secondary calibrators was fitted against time of day with a second-order polynomial, and this was then interpolated to correct the flux density for each observation in our program. The sky opacity was fairly constant during the first 30 hr of the observing run: at 450/800/1100 μm the zenity opacity ($\tau$) was 1.04/0.30/0.036 initially. Over the last 20 hr the opacity increased to a final value of 2.65/0.74/0.15 in the same three wave bands.

The set of observed flux densities were averaged for each galaxy, and the final results are listed in Table 2 along with the positions observed (at the nucleus of each galaxy). The uncertainties shown are those measured from the internal scatter of the data sample. We estimate that systematic uncertainties due to errors in the gain factor, the absolute flux of the calibrators, and scale errors in the sky opacity amount to a further 20%. For most of the observations listed in Table 2 the uncertainty is dominated by the internal errors. The galaxy types listed in Table 2 are taken from the catalog of *IRAS* fluxes by Knapp et al. (1989).

## 3. RESULTS

Detections of 3 $\sigma$ or better were obtained for only six of the 22 galaxies observed (NGC 205, NGC 404, NGC 1819, NGC 4383, NGC 4526, and NGC 6524). However, a further eight of the galaxies had sufficiently good data to set some interesting limits on dust temperatures and densities. The observed flux densities were combined with the *IRAS* measurements from Knapp et al. (1989) to obtain estimates of the dust temperatures. A power-law emissivity for the dust grains was used to calculate the emission at all wavelengths of interest, normalized to the JCMT data (see Fich & Hodge 1991 for more details of the methods used here). Figures 1*a*–1*n* show the *IRAS* data points, the JCMT data reported here (and listed in Table 2), and blackbody emission curves modified by power-law emissivities. The curve for the power-law index ($\beta$) 1.5 is highlighted and bracketed by fainter curves representing the emission expected for dust 2 degrees cooler or warmer. A separate curve is shown for a power-law index of 2.

The dust temperatures used to calculate the curves were found by iterating to find the best fits to the JCMT data and to the *IRAS* 100 and 60 μm data. In each case the temperature shown for the curve is an upper limit to the true dust temperature. The JCMT beam size is 15″–18″ depending on wavelength, while the *IRAS* beam sizes are much bigger (approximately 2′ and 4′ for the 60 and 100 μm points). Since the emission curves are normalized to the JCMT flux densities that come from a much smaller area on the sky, the dust temperatures are correct (rather than upper limits) only if all of the dust is within both the JCMT and *IRAS* beams.

TABLE 2

SUMMARY OF OBSERVATIONS

| NAME | TYPE | R.A.(1950) | DECL.(1950) | FLUX DENSITY (mJy) 1100 μm | 800 μm | 450 μm |
|---|---|---|---|---|---|---|
| NGC 185 ...... | dE3p | $00^h36^m12^s$ | 48°03′50″ | 8.2 ± 7.3 | ... | ... |
| NGC 205 ...... | E5p | 00 37 39 | 41 24 44 | 18.2 ± 3.9 | 10 ± 8 | −333 ± 513 |
| NGC 404 ...... | E/S0 | 01 06 39 | 35 27 10 | 24.7 ± 27.8 | 22 ± 7 | −86 ± 325 |
| NGC 632 ...... | S0 | 01 34 41 | 05 37 25 | −0.4 ± 17.7 | 33 ± 33 | 326 ± 298 |
| NGC 855 ...... | E | 02 11 10 | 27 38 36 | −32.7 ± 30.6 | 23 ± 11 | −314 ± 220 |
| UGC 2836 ..... | S0 | 03 40 39 | 39 08 14 | −1.2 ± 7.3 | ... | ... |
| NGC 1691 ..... | SB0a | 04 52 01 | 03 11 23 | 24.7 ± 14.6 | 55 ± 29 | −273 ± 514 |
| NGC 1819 ..... | SB0 | 05 09 06 | 05 08 28 | 35.8 ± 14.2 | 120 ± 77 | 714 ± 209 |
| NGC 2292 ..... | E/S0 | 06 45 39 | −26 41 24 | 8.2 ± 18.3 | −129 ± 88 | −1790 ± 2060 |
| NGC 2789 ..... | S0a | 09 12 01 | 29 56 18 | 7.1 ± 19.3 | −5 ± 37 | −163 ± 998 |
| NGC 3032 ..... | S0(3) | 09 49 14 | 29 28 20 | 18.1 ± 11.5 | 0 ± 29 | 642 ± 350 |
| NGC 3042 ..... | S0 | 09 50 46 | 0 56 08 | 43.4 ± 34.2 | ... | ... |
| NGC 3265 ..... | E4 | 10 28 19 | 29 03 13 | 1.2 ± 12.8 | 77 ± 30 | −687 ± 558 |
| NGC 3593 ..... | S0a | 11 11 59 | 13 05 28 | 31.2 ± 11.9 | 49 ± 64 | 190 ± 1088 |
| NGC 3928 ..... | E0 | 11 49 11 | 48 57 38 | 4.5 ± 15.9 | 4 ± 12 | 192 ± 122 |
| MGC 4383 .... | S0ap | 12 22 54 | 16 44 48 | 20.7 ± 9.0 | 51 ± 11 | 381 ± 209 |
| NGC 4526 ..... | S0(3) | 12 31 30 | 07 58 33 | 2.7 ± 26.3 | 55 ± 13 | 401 ± 300 |
| NGC 5506 ..... | I0 | 14 10 39 | −2 58 30 | 28.2 ± 31.6 | ... | ... |
| NGC 5784 ..... | S0 | 14 52 24 | 42 45 38 | 25.0 ± 8.6 | ... | ... |
| NGC 6524 ..... | E/S0 | 17 57 50 | 45 53 21 | −5.6 ± 18.9 | 129 ± 38 | ... |
| NGC 7464 ..... | E1p | 22 59 25 | 15 42 17 | ... | −24 ± 15 | ... |
| NGC 7465 ..... | SB0 | 22 59 32 | 15 41 50 | ... | −9 ± 13 | ... |

The dust temperatures can be combined with our submillimeter flux densities to calculate dust masses (again, see Fich & Hodge 1991 for more details). Since the temperatures are upper limits, the dust masses inferred are lower limits to the actual dust masses within each entire galaxy. The maximum temperatures and minimum masses are listed in Table 3 for each of the 14 galaxies where the data were good enough to give useful limits. Results for both power law indices are given. In all cases the $\beta = 1.5$ power-law gives a lower minimum mass, and we use that value in the discussion below. In general the temperature upper limits estimated here are lower than the temperatures obtained by use of only the *IRAS* 60 and 100 μm flux densities. In a number of cases the temperatures determined from the two calculations are similar. However, in two

TABLE 3

DERIVED LIMITS ON TEMPERATURE AND MEANS

| NAME | *IRAS* FLUX DENSITY (mJy) 100 μm | 60 μm | 25 μm | 12 μm | $\beta = 1.5$ $T_{max}$ (K) | $\beta = 1.5$ $M_{min}$ ($M_\odot$ Mpc$^{-2}$) | $\beta = 2.0$ $T_{max}$ (K) | $\beta = 2.0$ $M_{min}$ ($M_\odot$ Mps$^{-2}$) |
|---|---|---|---|---|---|---|---|---|
| NGC 185 ...... | 1720 | 440 | ... | ... | ... | ... | ... | ... |
| NGC 205 ...... | 3130 | 570 | 130 | 110 | 26 | 1853 | 22 | 4828 |
| NGC 404 ...... | 4000 | 2320 | 240 | ... | 36 | 502 | 28 | 1248 |
| NGC 632 ...... | 6510 | 5030 | 820 | 350 | 34 | 1346 | 27 | 2624 |
| NGC 855 ...... | 3270 | 1410 | ... | ... | 33 | 587 | 26 | 1445 |
| UGC 2836 ..... | 9970 | 470 | 500 | 330 | ... | ... | ... | ... |
| NGC 1691 ..... | 10450 | 7230 | 960 | 320 | 36 | 1597 | 26 | 5000 |
| NGC 1819 ..... | 12250 | 7360 | 790 | 320 | 34 | 2479 | 25 | 7619 |
| NGC 2292 ..... | 2460 | 390 | 70 | 130 | ... | ... | ... | ... |
| NGC 2789 ..... | 5490 | 2440 | 340 | 270 | ... | ... | ... | ... |
| NGC 3032 ..... | 4180 | 1990 | 260 | 250 | 30 | 1460 | 23 | 4292 |
| NGC 3042 ..... | 2580 | 340 | ... | ... | ... | ... | ... | ... |
| NGC 3265 ..... | 3690 | 2590 | 480 | 90 | 26 | 2704 | 21 | 6572 |
| NGC 3593 ..... | 35600 | 18870 | 2090 | 1310 | 42 | 1682 | 32 | 4877 |
| NGC 3928 ..... | 5150 | 3160 | 440 | 250 | 36 | 726 | 29 | 1371 |
| NGC 4383 ..... | 12650 | 8770 | 1140 | 320 | 39 | 1217 | 29 | 3652 |
| NGC 4526 ..... | 15200 | 5720 | 530 | 440 | 36 | 1255 | 29 | 2845 |
| NGC 5506 ..... | 8310 | 8790 | 4090 | 1300 | ... | ... | ... | ... |
| NGC 5784 ..... | 2560 | 790 | 70 | 60 | 25 | 2674 | 20 | 7146 |
| NGC 6524 ..... | 7900 | 3860 | 360 | 270 | 28 | 4093 | 22 | 10280 |
| NGC 7464 ..... | 6710 | 2500 | ... | ... | ... | ... | ... | ... |
| NGC 7465 ..... | 7300 | 3520 | 450 | 320 | ... | ... | ... | |

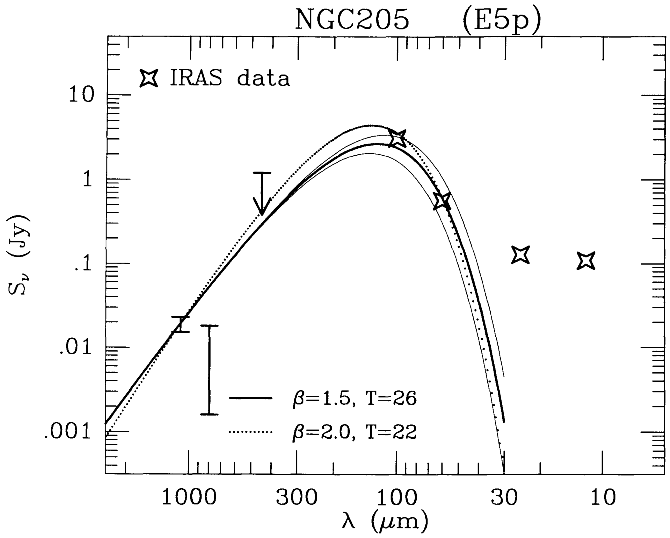


FIG. 1*a*

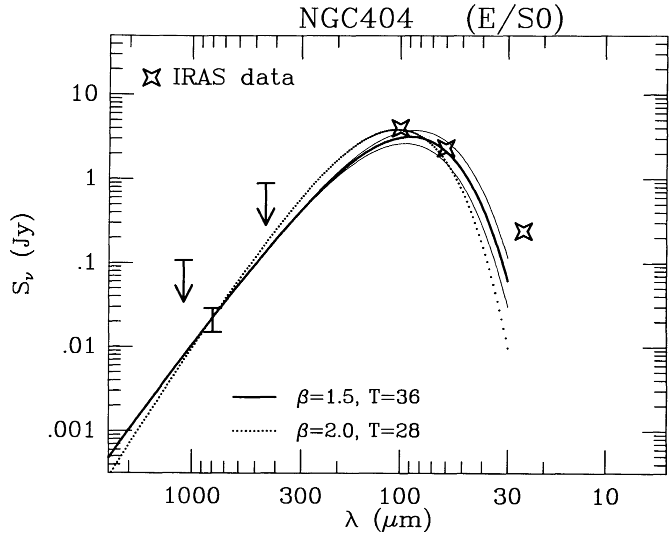


FIG. 1*b*

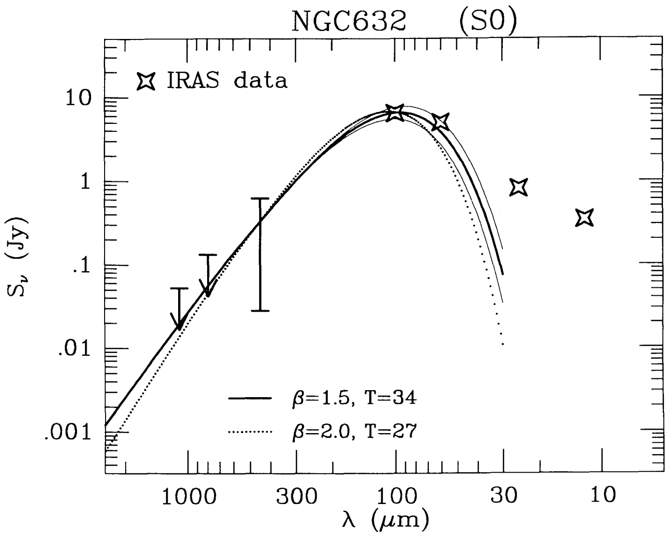


FIG. 1*c*

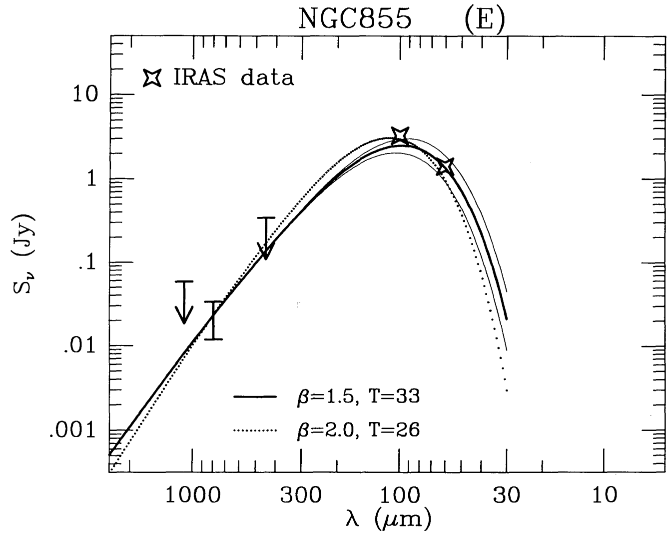


FIG. 1*d*

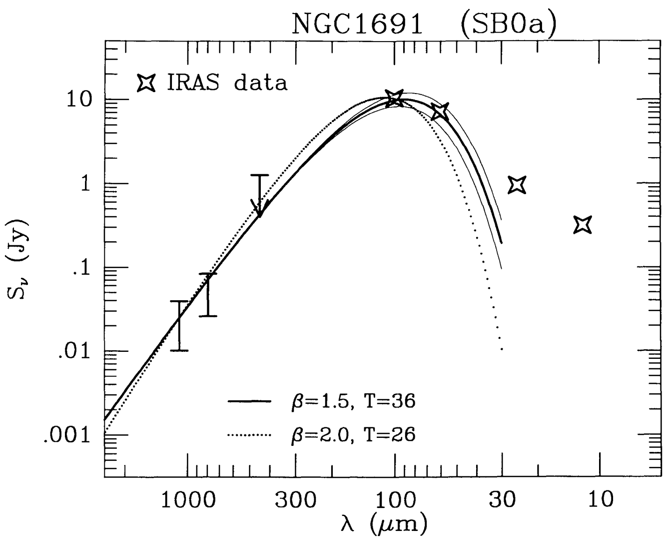


FIG. 1*e*

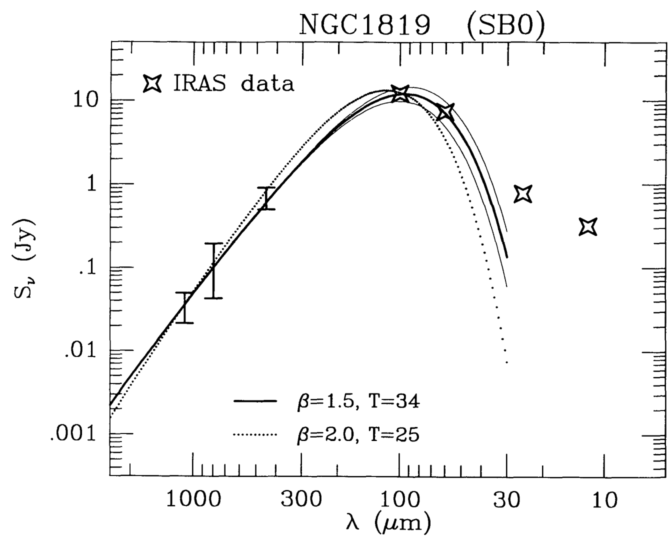


FIG. 1*f*

FIG. 1.—Observed flux densities are shown with 1 $\sigma$ uncertainties. The *IRAS* data points for 12, 25, 60, and 100 $\mu$m are shown by symbols that are larger than the measurement uncertainties (Knapp et al. 1989). The curves show models of the continuum emission for values of temperature and emissivity power-law index as labeled. The $\beta = 1.5$ power-law fit (*darkest solid line*) is bracketed by curves (*fainter lines*) 2 degrees cooler and warmer than the labeled curve. Another curve (*dotted*) shows the $\beta = 2$ best fit. (*a*) NGC 205, (*b*) NGC 404, (*c*) NGC 632, (*d*) NGC 855, (*e*) NGC 1691, (*f*) NGC 1819, (*g*) NGC 3032, (*h*) NGC 3265, (*i*) NGC 3593, (*j*) NGC 3928, (*k*) NGC 4383, (*l*) NGC 4526, (*m*) NGC 5784, (*n*) NGC 6524.

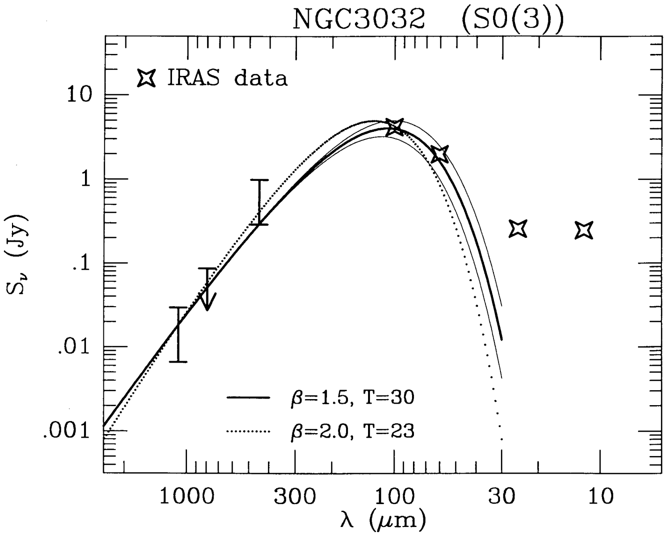


FIG. 1*g*

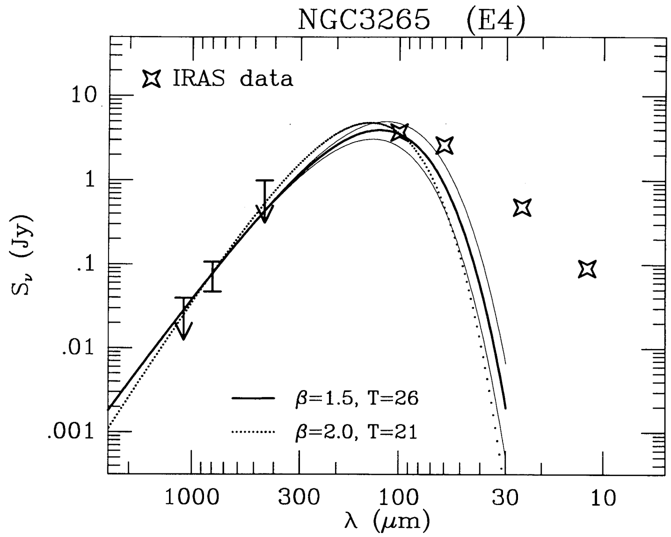


FIG. 1*h*

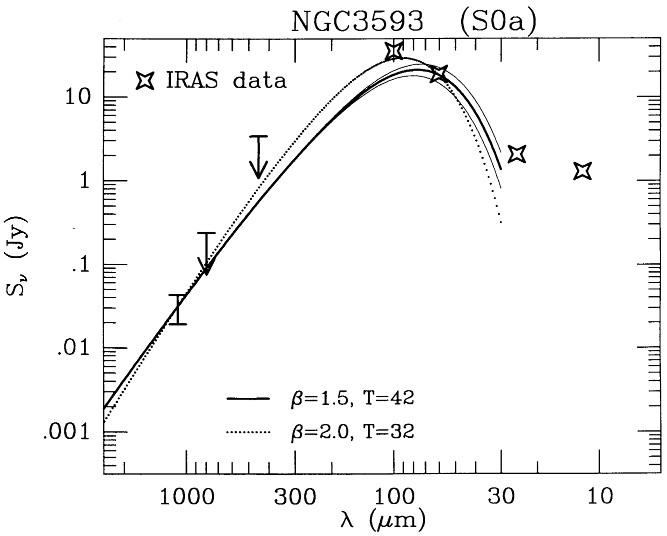


FIG. 1*i*

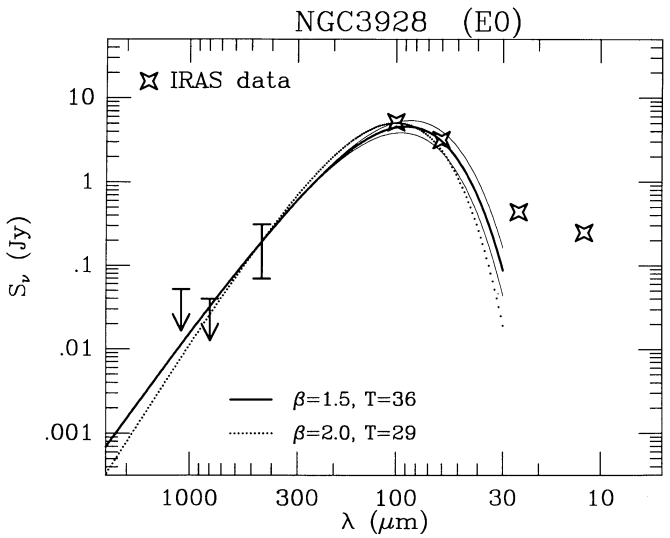


FIG. 1*j*

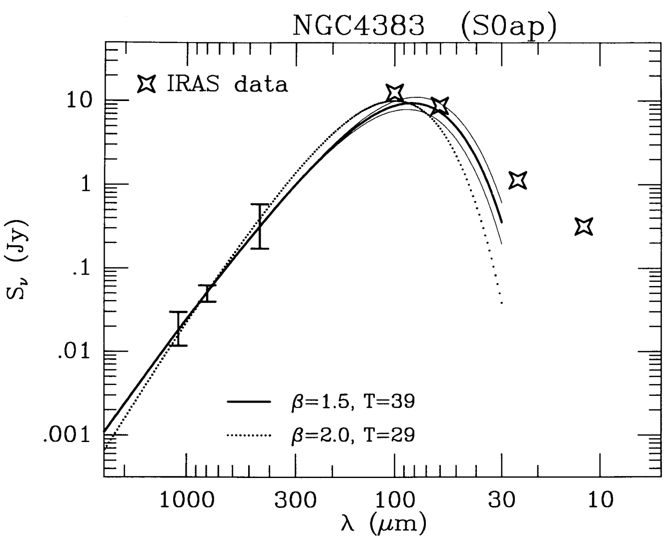


FIG. 1*k*

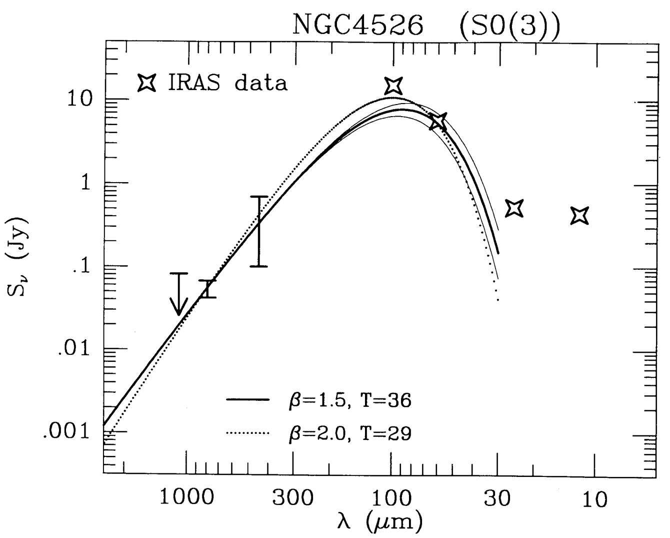


FIG. 1*l*

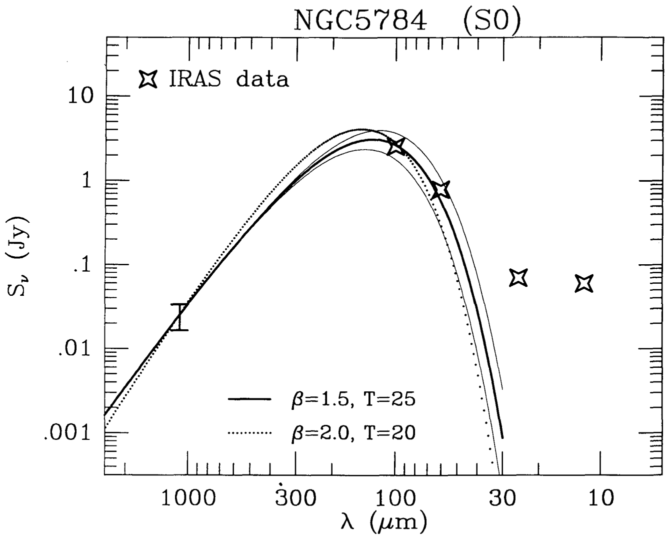


FIG. 1*m*

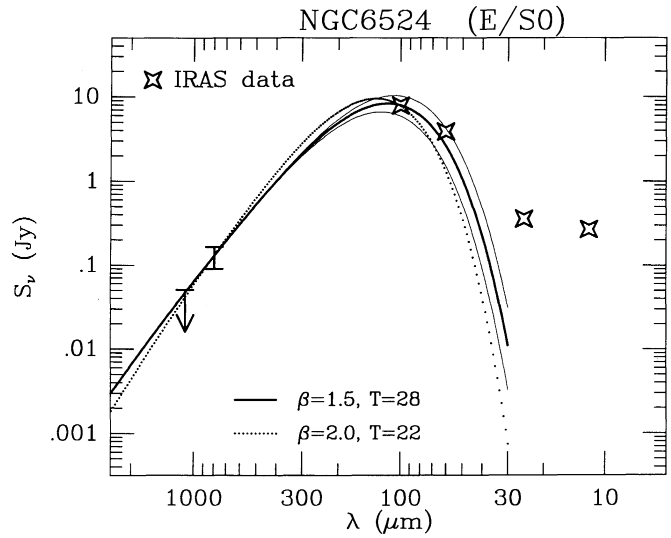


FIG. 1*n*

cases, NGC 3593 and NGC 4526, the *IRAS* temperature estimates are lower than our upper limits. These are the two brightest *IRAS* galaxies in our sample, and also among the largest in angular extent, and both factors probably play a role in causing this effect. For consistency throughout this paper we have used our upper temperature limit in calculating the dust-mass limits for all objects. The dust mass depends on the distance to the galaxy, but the entries in Table 3 are left in a distance-independent form in solar masses per unit distance (in Mpc) squared.

## 4. DISCUSSION

The ratio of gas to dust in our Galaxy is approximately 100 by mass and is similar in other spiral galaxies, such as M31 (Walterbos & Schwering 1987). Early-type galaxies, especially those of small mass, may have somewhat lower metallicities and might therefore have higher gas-to-dust ratios. There are only a small number of measurements of hydrogen content in early-type galaxies. We have used the compilations by Lees et al. (1991) and Roberts et al. (1991) to locate the H I and CO data discussed here. Out of the 14 galaxies in our set of "good detections," eight appear to have good H I detections and nine have good CO observations (used to estimate $M_{H_2}$ by scaling by the Milky Way conversion factor to estimate $H_2$ abundance). In Table 4 the total H I and $H_2$ masses (divided by distance squared) are shown for these galaxies. The values shown are those computed by Lees et al. (1991), if available; otherwise they are selected from Roberts et al. (1991). In each case the reference for the original observations is given in the following column. In column (6) of Table 4 the ratios of gas mass to (lower limit of) dust mass are shown. In several cases this upper limit on the gas-to-dust ratio approaches surprisingly closely the Galactic value of 100.

In all cases the H I and CO were observed with a much larger beam size than the JCMT beams of 15″–18″. If the H I and dust are uniformly distributed (or at least distributed in

TABLE 4

COMPARISONS WITH OBSERVATIONS AT OTHER WAVELENGTHS

| Name (1) | $M_{\rm H\,I}$ ($M_\odot$ Mpc$^{-2}$) (2) | Reference (3) | $M_{\rm H_2}$ ($M_\odot$ Mpc$^{-2}$) (4) | Reference (5) | $M_{\rm H}/(M_{\rm min})_{\rm dust}$ (6) | $d$ (Mpc) (7) | $M_B$ (8) | log $(M_{\rm min})_{\rm dust}/L_B$ ($M_\odot/L_\odot$) (9) |
|---|---|---|---|---|---|---|---|---|
| NGC 205 ...... | $7.6 \times 10^5$ | 1 | $7.3 \times 10^5$ | 9 | $8.0 \times 10^2$ | 0.7 | −16.0 | −5.63 |
| NGC 404 ...... | $1.0 \times 10^7$ | 2 | $1.1 \times 10^6$ | 10 | $2.2 \times 10^4$ | 3.1 | −15.8 | −4.83 |
| NGC 632 ...... | ... | ... | ... | ... | ... | 42.0 | −19.6 | −3.66 |
| NGC 855 ...... | $1.2 \times 10^6$ | 3 | $2.4 \times 10^4$ | 10 | $2.1 \times 10^3$ | 10.9 | −16.9 | −4.11 |
| NGC 1691 ..... | ... | ... | ... | ... | ... | 62.1 | −20.8 | −3.72 |
| NGC 1819 ..... | $6.8 \times 10^5$ | 4 | $2.5 \times 10^6$ | 11 | $1.3 \times 10^3$ | 59.3 | −20.2 | −3.33 |
| NGC 3032 ..... | $2.4 \times 10^5$ | 5 | $8.5 \times 10^5$ | 11 | $7.5 \times 10^2$ | 19.9 | −18.9 | −3.99 |
| NGC 3265 ..... | $4.2 \times 10^5$ | 6 | $2.5 \times 10^5$ | 10 | $2.5 \times 10^2$ | 18.4 | −17.2 | −3.11 |
| NGC 3593 ..... | $2.0 \times 10^6$ | 7 | $9.7 \times 10^6$ | 11 | $7.0 \times 10^3$ | 6.6 | −17.4 | −4.29 |
| NGC 3928 ..... | $1.7 \times 10^6$ | 8 | $9.5 \times 10^5$ | 12 | $3.7 \times 10^3$ | 14.0 | −17.6 | −4.08 |
| NGC 4383 ..... | ... | ... | ... | ... | ... | 22.5 | −18.6 | −3.84 |
| NGC 4526 ..... | ... | ... | $1.8 \times 10^6$ | 9 | $1.4 \times 10^3$ | 6.2 | −13.8 | −4.83 |
| NGC 5784 ..... | ... | ... | ... | ... | ... | 72.8 | −20.6 | −3.28 |
| NGC 6524 ..... | ... | ... | ... | ... | ... | 71.3 | −20.5 | −3.07 |

REFERENCES.—(1) Johnson & Gottesman 1983; (2) Baars & Wendker 1976; (3) Walsh et al. 1990; (4) Mirabel & Sanders 1988; (5) Giovanardi, Krumm, & Salpeter 1983; (6) Lake & Schommer 1984; (7) Huchtmeier 1982; (8) Thuan & Martin 1981; (9) Sage & Wrobel 1989; (10) Lees et al. 1991; (11) Thronson et al. 1989; (12) Jackson et al. 1989.

such a way that larger beam areas detect proportionally larger amounts of material), then the measured gas-to-dust ratio should be corrected by dividing each by the beam area used to make the measurement. For example, NGC 205 has both H I and CO measurements. The amounts are $7.6 \times 10^5$ $M_\odot$ $\text{Mpc}^{-2}$ of H I in a 2′ diameter beam (Johnson & Gottesman 1983) and $7.3 \times 10^5$ $M_\odot$ $\text{Mpc}^{-2}$ of $H_2$ in a 55″ beam (Sage & Wrobel 1989). The molecular hydrogen appears to have a much higher density near the center of NGC 205, and comparing the dust mass inferred ($1.9 \times 10^3$ $M_\odot$ $\text{Mpc}^{-2}$ in an 18″ beam) with the $H_2$ mass gives a gas-to-dust ratio of 41 after correcting for the effect of the different beam sizes (e.g., estimating the surface density ratio of the $H_2$ to the dust). While this is even lower than the Galactic value, the many uncertainties inherent in this estimate suggest that this difference should not be considered significant. Nevertheless, since all of the gas measurements use beam sizes larger than the JCMT dust measurements, the same arguments could be used for the other galaxies, and therefore our inferred gas-to-dust ratios are likely higher than the real values because of this effect.

In columns (4) and (5) of Table 4 the distances and absolute blue magnitudes ($M_B$) for each galaxy are given, based on a value for the Hubble constant of 75 km $\text{s}^{-1}$ $\text{Mpc}^{-1}$ and using the apparent magnitudes from Knapp et al. (1989). The logarithms of the ratio of the dust mass (actually the lower limit on the dust mass in $M_\odot$) to the blue luminosity (in $L_\odot$) are shown in the final column of Table 4, where $M_B(\text{Sun}) = 5.48$ was used to calculate the luminosities. The luminosity given is that of the entire galaxy in each case. However, the observations of the dust mass are only taken from the central region. If there are significant amounts of dust farther from the centers of these galaxies, then these values are even more emphatically lower limits to the actual ratio. Correcting for the different angular scales of the different observed quantities is quite difficult, since the relative distribution of each of these components is not known. Most authors have chosen to follow the route of making the best estimate of the total (i.e., global) value of each characteristic, and we do the same.

Bregman et al. (1992) have shown that on average the ratio of dust mass to blue luminosity is below $-5$ for elliptical galaxies (both E and E/S0 types), rising to approximately $-4.7$ for S0 (2 and 3) and S0/Sa galaxies, and $-4.2$ for Sa galaxies in their sample of bright galaxies. The values found for our galaxies span a much larger range, from below $-5$ for the Local Group elliptical galaxy NGC 205 to $-3.11$ for the elliptical galaxy NGC 3265 and $-3.28$ for the S0 galaxy NGC 5784.

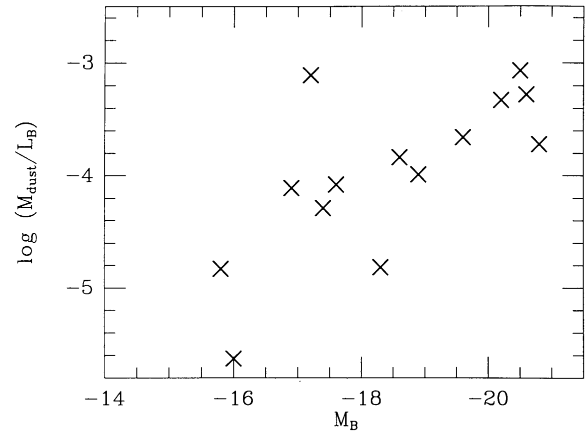


FIG. 2.—Ratio of (lower limit of) dust mass to blue luminosity of each galaxy plotted against absolute blue magnitude ($M_B$).

The latter values are quite high and suggest that these galaxies would be good candidates for further work. However, late-type spiral galaxies, on average, have $\log (M_{\text{dust}}/L_B) = -2$, an order of magnitude greater than these dusty early-type galaxies. Figure 2 shows the dust mass-to-light ratio plotted against $M_B$. There is a correlation evident in that the brightest galaxies seem to have higher ratios of dust to light but the scatter in the correlation is large. We have not yet investigated all of the sources of bias in this sample, and thus it is too soon to declare whether or not this correlation is significant.

In summary, the gas-to-dust ratios determined from these observations are higher than those measured in our Galaxy, but the entire difference can be easily due to differences in the beam sizes of the instruments used. Furthermore, our observations only give lower limits on the amount of cold dust. Thus the data are entirely consistent with identical gas-to-dust ratios. The amounts of dust detected are consistent with the presence of large amounts of cold dust compared with the amounts of warm dust.

M. F. has been supported in this work by the Natural Science and Engineering Research Council (Canada) through an Operating Grant and a Travel Grant (administered by the National Research Council). P. H. acknowledges support from National Science Foundation grant AST 88-14526.

## REFERENCES


Baars, J. W. M., & Wendker, H. J. 1976, A&A, 48, 405
Bregman, J. N., Hogg, D. E., & Roberts, M. S. 1992, ApJ, 387, 484
Cox, P., & Mezger, P. G. 1989, Astron. Astrophys. Rev., 1, 49
Duncan, W. D., Robson, E. I., Ade, P. A. R., Griffin, M. G., & Sandell, G. 1990, MNRAS, 243, 126
Ebneter, K., & Balick, B. 1985, AJ, 90, 183
Fich, M., & Hodge, P. 1991, ApJ, 374, L17
Giovanardi, C., Krumm, N., & Salpeter, E. E. 1983, AJ, 88, 1719
Griffin, M. J., Ade, P. A. R., Orton, G. S., Robson, E. I., Gear, W. K., Nolt, I. G., & Radostitz, J. V. 1986, Icarus, 65, 244
Huchtmeier, W. K. 1982, A&A, 110, 121
Jackson, J. M., Snell, R. L., Ho, P. T. P., & Barrett, A. H. 1989, ApJ, 337, 680
Johnson, D. W., & Gottesman, S. T. 1983, ApJ, 275, 549
Jura, M. 1986, ApJ, 306, 483
Knapp, G. R., Guhathakurta, P., Kin, D.-W., & Jura, M. 1989, ApJS, 70, 329
Knapp, G. R., Turner, E. L., & Cuniffe, P. E. 1985, AJ, 90, 454
Lake, G., & Schommer, R. A. 1984, ApJ, 280, 107
Lees, J. F., Knapp, G. R., Rupen, M. P., & Phillips, T. G. 1991, ApJ, 379, 177
Matthews, H. E. 1990, The James Clerk Maxwell Telescope: A Guide for the Prospective User (Hilo: Joint Astronomy Centre)
Mirabel, I. F., & Sanders, D. B. 1988, ApJ, 335, 104
Roberts, M. S., Hogg, D. E., Bregmann, J. N., Foreman, W. R., & Jones, C. 1991, ApJS, 75, 751
Sage, L. J., & Wrobel, J. M. 1989, ApJ, 344, 204
Thronson, H. A., Tacconi, L., Kenney, J., Greenhouse, M. A., Margulis, M., Tacconi-Garman, L., & Young, J. S. 1989, 344, 747
Thuan, T. X., & Martin, G. E. 1981, ApJ, 247, 823
Walsh, D. E. P., van Gorkom, J. H., Bies, W. E., Katz, N., Knapp, G. R., & Wallington, S. 1990, ApJ, 352, 532
Walterbos, R., & Schwering, P. 1987, A&A, 180, 27
Wardle, M., & Knapp, G. R. 1986, AJ, 91, 23
Wilcots, E. M., Hodge, P., Eskridge, P. B., Bertola, F., & Buson, L. 1990, ApJ, 364, 87
Young, J. 1990, in The Interstellar Medium of Galaxies, ed. H. A. Thronson, Jr., & J. M. Schull (Dordrecht: Kluwer), 67